DYNAMICS OF THE RECIRCULATING AREAS OF A FORWARD-FACING-STEP

Anthony Graziani
LAMIH CNRS UMR 8201,
University of Valenciennes
Campus Mont Houy, 59313 Valenciennes Cedex, France.
anthony.graziani@etu.univ-valenciennes.fr
&
Institut de Recherche Technologique Railenium
F-59300, Famars, France
anthony.graziani@railenium.eu

Franck Kerhervé
Institut PPRIME - UPR 3346
CNRS - University of Poitiers - ENSMA
Dept. Fluides, Thermique, Combustion
Poitiers, France
franck.kerherve@univ-poitiers.fr

Marc Lippert, Laurent Keirsbulck, David Uystepruyst
LAMIH CNRS UMR 8201,
University of Valenciennes
Campus Mont Houy, 59313 Valenciennes Cedex, France.
laurent.keirsbulck@univ-valenciennes.fr

Robert J. Martinuzzi
Dept. Mechanical & Manufacturing Eng.
University of Calgary
2500 University Dr. NW
Calgary, Alberta, Canada
rmartinu@ucalgary.ca

ABSTRACT

The dynamics of the velocity and surface pressure fields in the recirculating regions upstream of the foot of a forward-facing step and downstream of the step corner are investigated experimentally for a thin turbulent oncoming boundary layer at a Reynolds number, based on the step height, of 10^5. Velocity measurements are acquired concurrently in the upstream and downstream regions of the step using Particle Image Velocimetry (PIV) and synchronized with time-resolved wall-pressure measurements acquired at 20 locations on the front and top walls of the step. A multi-time-delay linear stochastic estimation is employed to reconstruct time-resolved PIV snapshots to reveal the nature of the connection between the upstream and downstream recirculating regions. It is shown that the complex dynamics of the upstream recirculating bubble is imprinted onto the separated flow region on the top of the step.

1 INTRODUCTION

The two-dimensional forward-facing step (FFS) is a heuristic geometric simplification for studying the inception and propagation of fluid instabilities for prismatic bodies. In practice, such instabilities are often the root cause for undesirable engineering outcomes including reduced material life – *e.g.* fatigue failure due to tarpaulin flapping on heavy transport vehicles, or structural damage and debris dispersal as observed for low-lying-building roofs.

The flow over a FFS is made particularly complex due to the formation of dual recirculation regions as depicted in Fig. 1. When approaching the step, the flow experiences increasing adverse pressure gradient and the incoming boundary layer separates only $\sim$1-2 step heights upstream the step. A recirculation region forms at the foot of the step, with reattachment on the face of the step. The flow then experiences separation again due to the leading step's edge while reattaching further downstream. Both separation regions are continuously exposed to incoming perturbations and natural unsteadiness of the surrounding flow resulting in large wall-pressure fluctuations on the different walls of the steps (Largeau & Moriniere, 2007; Camussi *et al.*, 2008; Sherry *et al.*, 2010). In the downstream recirculation region on the top of the step, the mean reattachment length depends on a variety of flow parameters such as the freestream turbulence level (Hillier & Cherry, 1981), the incoming boundary layer thickness to step heigh ratio δ/H (Sherry *et al.*, 2010; Pearson *et al.*, 2013), or again the Reynolds number (Largeau & Moriniere, 2007). Following Sherry *et al.* (2010), the flow over FFS can be classified into steps being submerged in the incoming boundary layer ($\delta/H < 1$) and conversely steps with ratio $\delta/H > 1$. For immersed steps, the dynamics of the downstream separation region is known to be strongly affected by the incoming boundary layer (Farabee & Casarella, 1986*a*).

Pearson *et al.* (2013) recently suggested that the unsteady separation events observed just upstream of the step may be strongly influences by the large-scale structures embedded in the outer part of the oncoming boundary layer. The authors characterised the dynamics of the upstream separation region in terms of random fluctuation in its size punctuated by cyclical but aperiodic bursting events, in which the entire recirculation region is suddenly evacuated over the step. These dynamics have been found to be potentially altered through disturbances of the oncoming boundary layer.

The understanding of the influence of the oncoming flow conditions on the dynamics of the recirculation regions remains however fragmented. This is due to, in part,

the poorly understood but strong coupling between the upstream and downstream recirculation regions and the still incompletely described dynamics of the upstream recirculation bubble. In this work, the dynamics of the upstream recirculation bubble are investigated for a turbulent but thin boundary layer, $\delta/H \approx 0.49 < 1$, which is more characteristic of transport applications. The coupling between the dynamics of top separated flow and upstream region is then explored and discussed.

2 EXPERIMENTAL SET-UP

2.1 Wind-tunnel and Geometry

Experiments were conducted in the LAMIH wind tunnel facility. Full details of the wind-tunnel and of its characterization can be found in Keirsbulck *et al.* (2012). The test vein section is 2×2 m^2, 10 m long. The vertical walls are made in perspex for optical access. The wind tunnel inlet generates a turbulence intensity less than 0.6% of the free-stream velocity U_∞. For the present work, a forward facing step was installed vertically on one side of the wind tunnel test section at a distance of 4.17 m from the inlet. The model, made in wood, spans the entire height of the wind tunnel. The height of the step, H, is 0.166 m. While different Reynolds numbers have been investigated, only the results for $Re_H = 1.14\times10^5$ are discussed here. The corresponding free stream velocity is $U_\infty = 10$ m/s.

The oncoming boundary layer profile, measured at a distance $2.11H$ upstream of the step was measured using a Pitot tube. At this location, the boundary layer is fully turbulent and fits well with the theoretical one-seventh power law. The boundary layer thickness, δ, was estimated to be 0.082 m, resulting in $\delta^\star = \delta/H \approx 0.493$. The displacement thickness δ_1 and the momentum thickness θ are 6.6 mm and 5.5 mm respectively. The Reynolds number based on the momentum thickness is $Re_\theta \approx 3785$. The present configuration is thus noticeably different from the major studies reported in the literature for which the step was submerged into the boundary layer ($\delta^\star > 1$) (Castro & Dianat, 1983; Camussi *et al.*, 2008). As stated in the introduction, the choice of $\delta^\star \leq 1$ is motivated by concerns related to transport system. Unsteady perturbations of the oncoming boundary layer were for long thought to play an active role on the dynamics of the flow surrounding the step Sherry *et al.* (2010), and were shown recently by Pearson *et al.* (2013) to drive the dynamics of the separation region occurring just upstream of the step. Lower values of $\delta^\star$ are believed to make the dynamics of this upstream region more robust to the oncoming perturbations and to make the main flow characteristics less Reynolds dependent (Ren & Wu, 2011; Pearson *et al.*, 2013).

2.2 Velocity and Pressure Measurements

A two-component classical Particle Image Velocimetry (PIV) system was used to map the velocity field upstream and over the step along the centre-plane. The PIV system includes a 250 mJ double-pulsed Yag Laser (wavelength 532 nm) and two high resolution TSI Powerview cameras of 2048×2048 pixels each. The measurement plane covers continuous regions upstream and downstream of the step as depicted in Fig. 1. The laser sheet is 5 mm thick. The time interval between two consecutive image-frames was 50 μs. Instantaneous velocity vectors in the x–y plane were estimated from the particle displacement within an image pair using a conventional direct cross-correlation process including multi-pass windows to validate the vectors using a 5×5 median test. A bad-vector-replacement step is provided by using a 5×5 median interpolation method, concluded by a low-pass filter process to avoid PIV noise. The resulting fields have a final resolution $\Delta x = \Delta y = 0.9924$ mm. The final data-set includes 2000 PIV snapshots sampled at $f_{\mathrm{PIV}} = 7Hz$.

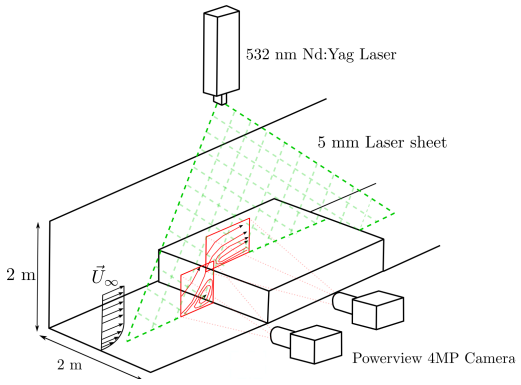

Figure 1. Schematic of the experimental set-up.

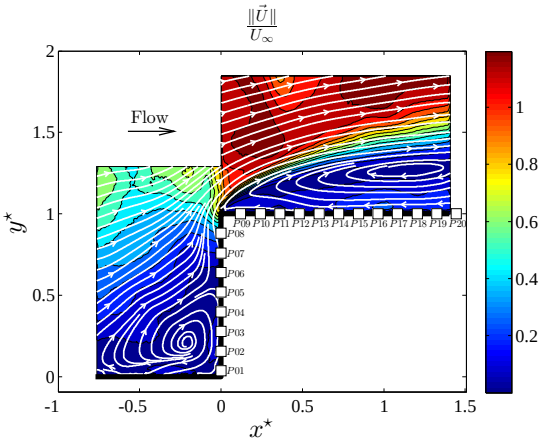

Figure 2. Mean velocity field over FFS. Contours coloured by magnitude of velocity. White squares indicate pressure sensor locations.

Surface pressure measurements are obtained at 20 locations along the front and top walls of the step using flush-mounted sensors. Eight sensors (#P01-#P08) are located on the front side of the step while twelve (#P09–#P20) are located on the top of the step as depicted in Fig. 2. The pressure transducers are commercial KULITE-XCP-062 calibrated by the manufacturer. The sensors are spaced uniformly $0.12H$ apart. Pressure signals were recorded at a sampling frequency of $f_s = 10$ kHz and are low pass filtered using an 8^{th} order Bessel filter with cut-off frequency $f_{cutt} = 3$ kHz. In order to avoid reflections with the PIV laser sheet, the sensors are offset spanwise 2 mm from the PIV measurement plane.

3 RECIRCULATING REGIONS

The time-averaged velocity fields and the wall-pressure energy spectra are first examined to identify the main flow features and more particularly to identify the dominant frequencies driving the dynamics in the different flow regions.

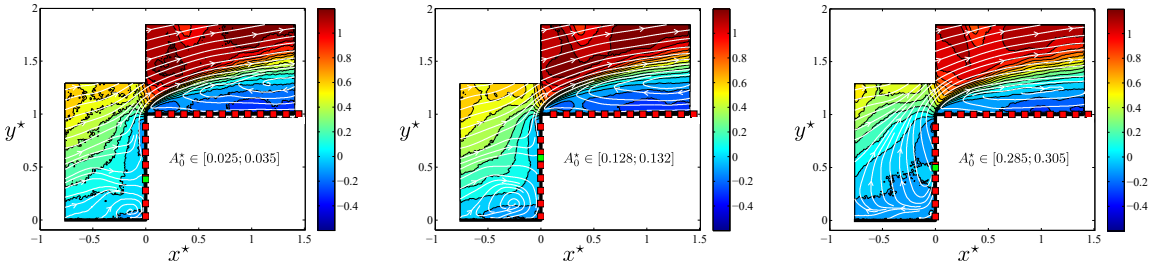

(a) (b) (c)

Figure 4. Conditional averaging velocity fields superimposed with streamlines for different values of A_0^* refereed in the PDF. The green square represent the position of the stagnation/reattachment point.

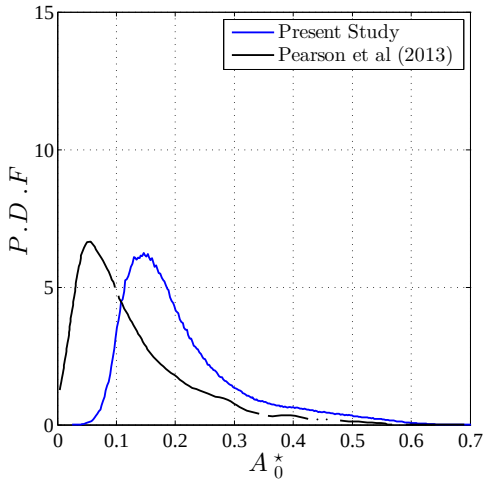

Figure 3. Probability density function of the reverse flow area upstream of the step: (Blue line) Present data, (black line) Pearson et al (2013).

3.1 Mean flow field

The mean velocity flow field is reported in Fig. 2. As expected, two recirculating regions are observed: one upstream at the foot of the step and the other over the top wall downstream of the step. For the upstream one, the mean separation point is slightly upstream of the PIV domain. Results from the literature suggest that the location of the separation point along the upstream wall and that of the reattachment point on the front face are independent of the Reynolds number (Addad *et al.*, 2003; Camussi *et al.*, 2008). In the present results, the separation point can be estimated to occur $\sim 1H$ upstream of the step, while the reattachment point on the front side is found to be $\sim 0.55H$ from the bottom wall, which is good agreement with earlier results (Leclercq *et al.*, 2001; Sherry *et al.*, 2009). When passing the step's corner, the flow separates again due to the sharp edge (locally high curvature). While not detailed here, the mean reattachment location was found to be $3.2H$ downstream of the step, outside of the current PIV domain, which is well consistent with the literature (Largeau & Moriniere, 2007).

3.2 Agitated life of the upstream region

Examination of instantaneous PIV snapshots reveal that the upstream region is highly unsteady. The size of the reverse flow region varies significantly. It can reach stages where the reverse flow extends above the step height or can at certain instances almost vanish.

To obtain a finer description of the flow allowing investigation of the unsteady behaviour of the recirculation region from the present PIV measurements, a time-resolved estimation of the flow field is undertaken to take advantage of the high sampling rate of the pressure sensors. Here an adaptation of the linear stochastic estimation (LSE) technique of Adrian (1977) is used. Briefly, the LSE is a linear approximation of the conditional estimate of some quantity as obtained given a set of observables. Here, the conditional variables (the quantities to estimate) are the fluctuating velocity components as measured with PIV, while the set of observables (*i.e.* the estimators) are the pressure fluctuations measured along the wall.

To account for the lag between the velocity and pressure fields sampled at different locations, a multi-time formulation as described by Murray & Ukeiley (2003) or Kerhervé *et al.* (2012) is implemented in which $N_j - 1$ virtual sensors and 1 physical sensor, each delayed by one acquisition interval Δt_a to the previous, are introduced such that the sensor specific delay is $\tau_{jk} = (k-1)\Delta t_a$. The LSE is then defined over the $N = 20$ sensors for each veloicty component at each point of the PIV plane according to:

$$\hat{u}_i(x,y,t) = \sum_{k=1}^{N} \sum_{j=1}^{N_j} \alpha_{jk}^{(i)} p(X_k, Y_k, t - \tau_{jk}) \ , i = 1,2$$

where u_i denotes the i-th velocity component, X_k, Y_k the location of the physical sensor and the estimator coefficients $\alpha_{jk}^{(i)}$ are determined by minimising the residual error $\|u_i(x,y,t) - \hat{u}_i(x,y,t)\|^2$ defined in the L_2 norm sense. The parameters Δt_a and N_j were selecting after examination of the temporal velocity-pressure correlations. For clarity, the estimations will be referred to as time-resolved reconstructed PIV snapshots.

Using these reconstructed PIV snapshots, time history of the area of the upstream reverse flow region, noted $A_0(t)$, is computed as,

$$A_0(t) = \int_{\Omega_{x<0}} \mathscr{H}\{\tilde{u}(\mathbf{x},\mathbf{t})\} \ \mathbf{dx} \qquad (1)$$

with $\tilde{u}(\mathbf{x},\mathbf{t})$ the estimated streamwise velocity component, and $\mathscr{H}$ the Heaviside function defined by,

$$\mathscr{H}(X) = \begin{cases} 0 \text{ if } X \geq 0 \\ 1 \text{ if } X < 0 \end{cases} \qquad (2)$$

The spatial domain $\Omega_{x<0}$ denotes the flow region upstream

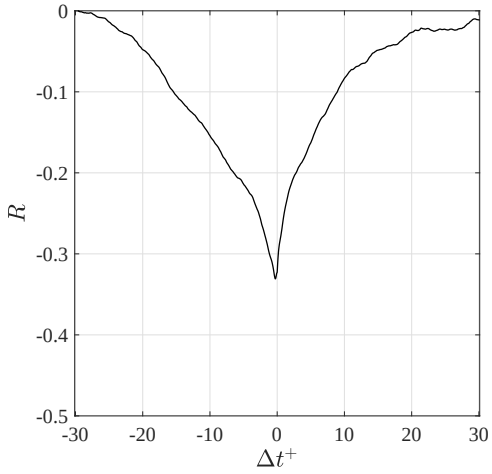

Figure 5. Normalised cross-correlation function between upstream and downstream recirculating region area A_0 and A_1 respectively.

of the step. The probability density function of $A_0^* = A_0/H^2$ is shown in Fig. 3 with that reported by Pearson *et al.* (2013) for a fully immersed forward facing step ($\delta/H > 1$) but with similar Reynolds number. The present result shows a right tail shape distribution, similar to that observed by Pearson *et al* but shifted towards higher values. An approach similar to that of Pearson *et al* is now used to examine the state of the flow for selected values α of A_0. The time-resolved reconstructed velocity snapshots for which the upstream reverse flow area A_0 is comprised in $[\alpha-\varepsilon, \alpha+\varepsilon]$ are identified and averaged together. The coefficient ε allows conditioning over a small range of A_0 to ensure statistical convergence.

Conditionally averaged velocity snapshots for different values of α are plotted in Fig. 4 and are representative of the different stages of the flow at the foot of the FFS. The conditionally averaged field for the peak value of the probability density function (pdf), i.e. the value with the most occurrence, is reported in Fig. 4(b) and shows strong resemblance with the mean field. Here, the upstream separated flow region is a "closed-type" with a reattachment point on the step frontal face. The formed bubble acts like a ramp deviating the oncoming flow above the step corner. In Fig. 4(a), the upstream flow region is close to an "open-type" configuration such as described by Lanzerstorfer & Kuhlmann (2012) (amongst others). The separation region upstream of the step exhibits a small recirculation bubble just at the foot of the step but does not exhibit a reattachment point on the step face. In this configuration, part of the incident flow rolls into a vortex at the step's foot. In contrast, Fig. 4(c) shows a configuration of "massive separation". The flow just upstream the step acts like a fence by preventing the oncoming flow from impacting on the step's face. Such events have been referred as streak by Stüer *et al.* (1999).

Close examination of the time-resolved reconstructed PIV snapshots allows to envisage the following scenario: an upstream recirculating bubble at the step's foot of open-type first starts to grow in size (figure 4(a)), reaching rapidly the median stage (Fig. 4(b)). The accumulation of dynamic pressure and vorticity over the bubble then reinforces the reverse flow area until saturation where the energy accumulated is released over the step (Fig. 4(c)) allowing the formation of a new upstream recirculating bubble at the step's foot.

While the upstream flow region at the step's foot exhibits an agitated life as described above, it is noteworthy that the downstream separation region appears to show less complex dynamics. Based on observations over the entire reconstructed sequence: while successive cycles of the scenario given above are observed, the downstream recirculating bubble shows essentially a slow (flapping) motion in the wall-normal direction. However, the flapping motion shows some synchronisation with the upstream dynamics and is modified by events in the upstream region. The connection between both recirculating regions is examined in the following section.

4 CONNECTION OF THE TWO RECIRCULATING REGIONS

4.1 Synchronisation

Time history of the downstream separation area A_1 can be computed similarly to that of the upstream region using Eq. (1). A preliminary indication of the nature of the connection between the upstream and downstream recirculating regions is given by the cross-correlation function between the two areas reported in Fig. 5.

A correlation peak at a time delay $\Delta t^+ \simeq -0.26$ with negative value of -0.33 is observed. This indicates that both recirculating flow regions are strongly linked and that most of the time evolve in opposite phase: an increase in the upstream reverse flow region entrains a decrease of the downstream within a relatively short time delay. While not shown here, the time-resolved reconstructed field exhibits a similar tendency. The significant but low correlation value also suggests that the connection probably occurs through non-linear phenomena, motivating a further analysis to understand the mechanism underlying the connection.

4.2 Wall-pressure fluctuations

Wall-pressure energy spectra along the front and top sides of the step are reported in Fig. 6. The spectra are non-dimensionalised for readability The overall energy spectra reveal two dominant broadband frequency regions : (i) a low-frequency region centred on $St_H = fH/U_\infty \simeq 0.02$ identified along both the front and top side of the step, (ii) a moderate-frequency region for which the peak frequency is varying from $St_H \simeq 1$ to $St_H \simeq 0.2$ when moving downstream the top of the step. The latter is observed for the wall-pressure sensors on top side of the step only, and must be associated with the slow flapping of the separated downstream shear-layer and the shedding of eddies originating at the step corner (Farabee & Casarella, 1986*b*).

The low-frequency broadband activity is, in contrast, observed for all wall-pressure sensors. On the bottom wall just before the step, wall-pressure fluctuations are known to be driven by the onset of large scale dynamics and by the unsteadiness of the oncoming boundary layer turbulence (Awasthi *et al.*, 2014; Camussi *et al.*, 2008). In the present configuration, the wall-sensors are located directly on the face of the step. When moving from the bottom of the step (sensor #P01) towards the step's corner (sensor #P08), the energy of the broadband peak increases significantly. The broadband peak is centred around $St_H = 0.02$. When passing the step's corner, the amplitude of the peak increases significantly, while the spectral content is enriched with frequencies centred around $St = 0.03$. Further downstream along the top wall, the large amplitude of this low-frequency broadband peak persists over a long distance up

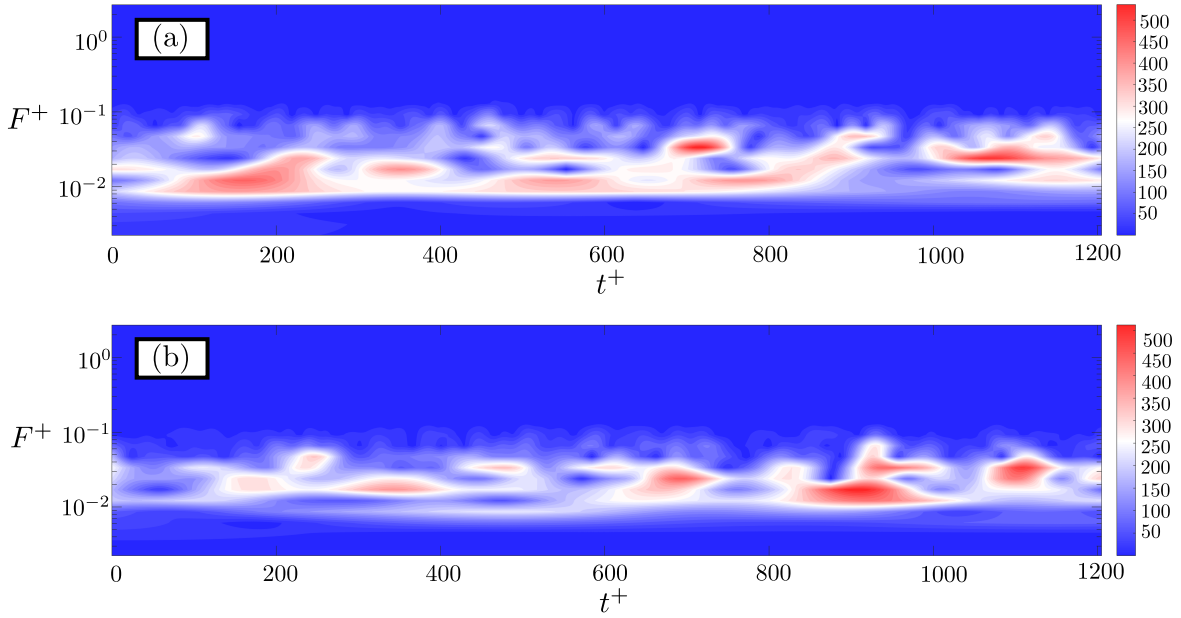

Figure 7. Wavelet spectra for wall-pressure sensors (a) #P08 located just upstream the step's corner on the front side, (b) #P09 located just downstream the step's corder on the top wall. See figure 2 for exact location of the sensors.

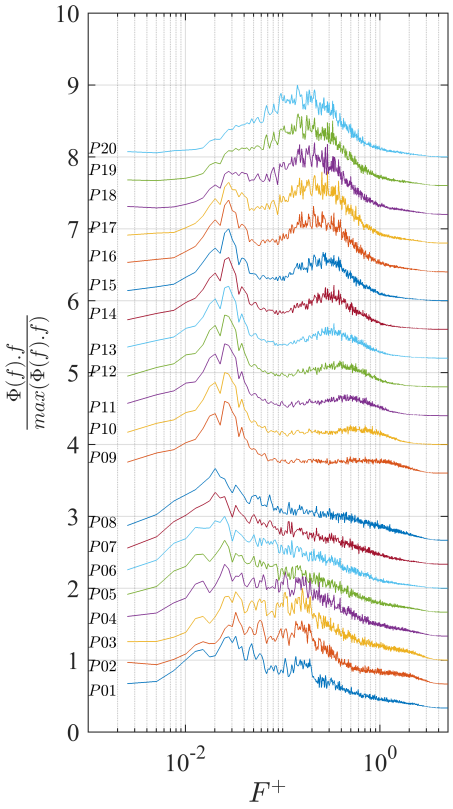

Figure 6. Normalised pre-multiplied wall-pressure fluctuations spectra. The results are shifted vertically for readability.

to about one step height downstream of the corner before reducing.

Of particular interest is the frequency peak at $St_H = 0.02$ originating from the upstream separating region which persists far downstream the step's corner while coexisting with frequencies close to $St_H = 0.03$ originating from the step's corner. These results must however be examined with care. In fact, while not reported here for brevity, wall-pressure energy spectra computed over shorter durations reveal that the two low-frequency peaks are not always present together. This suggests that the low-frequency dynamics driving the upstream recirculating region is strongly time-dependent. A time-dependent spectral analysis of the wall-pressure time-series is thus performed using wavelets.

The wavelet spectra of the two sensors #P08 and #P09 located on each side of the step's corner are reported in Fig. 7 for an arbitrary, representative time sequence. Note that for clarity, the wall-pressure time-series have been filtered to highlight the low-frequency activity only. Sudden changes in the dominant frequency is evident during the sequence shown. In the low-frequency band, the energy of the wavelet spectra is found to exhibit short time intervals where the two low frequencies discussed previously are at play simultaneously. Other time intervals show only one of the two frequencies and short periods in which the wall-pressure fluctuations are driven by a frequency caught in between.

Thanks to the time-resolved reconstructed PIV snapshots, it is possible to compute conditionally-averaged snapshots based on the wavelet spectra discussed here. For the periods of time where the wavelet spectra show a frequency caught in between, the velocity field is characterised by the "blow-up" of the upstream separation region described in §3.2. During this particular instant, the large amount of energy and vorticity accumulated in the upstream recirculating region is evacuated downstream the step, allowing direct communication between the upstream and downstream sides of the step's corner. In contrast, during the period when the two frequencies co-exist, the conditionally-averaged snapshots show resemblance with figure 4(b) with a large upstream separation region with reattachment point on the step's face. The two distinct frequencies may be attributed to flapping motions of the up-

stream and downstream recirculating regions respectively behaving mostly in opposite phase as discussed in §4.1.

5 CONCLUSION

The nature of the interactions between the upstream and downstream recirculating regions of a forward-facing step at high Reynolds number has been examined in details thanks to extensive flow (PIV) and wall-pressure surveys. The complex dynamics of the upstream separated region is found to imprint onto that of the separated region just downstream the step's corner. Conditional averaging based on the upstream separation area and on the wavelet analysis of the wall-pressure fluctuations revealed that the dynamics of the separated shear-layer is locally influenced by the low-frequency unrest of the upstream recirculating region at the step's foot while being globally dominated by Kelvin-Helmholtz instability. These interactions occur through a very limited range of time-varying low-frequencies driving the formation and blowing-up of a region of high vorticity at the step's foot. The exact nature of the non-linear interactions remains however unknown and further works will address this specific question.

Acknowledgements

The present work has been supported by Campus International pour la Sécurité et l'Intermodalité des Transports, la Région Nord-Pas-de-Calais, l'Union Européenne, la Direction de la Recherche, Enseignement Supérieur, Santé et Technologies de l'Information et de la Communication et le Centre National de la Recherche Scientifique. The authors gratefully acknowledge the support of these institutions.

REFERENCES

Addad, Y., Laurence, D., Tallotte, C. & Jacob, M.C. 2003 Large eddy simulation of a forward-backward facing step for acoustic source identification. *International Journal Heat and Fluid Flow* **24**, 562–571.

Adrian, R. J. 1977 On the role of conditional averages in turbulence theory. *Turbulence in Liquids* **1**, 323–332.

Awasthi, M., Devenport, W. J., Glegg, S. A. L. & Forest, J. B. 2014 Pressure fluctuations produced by forward steps immersed in a turbulent boundary layer. *Journal of Fluid Mechanics* **756**, 384–421.

Camussi, R., Felli, M., Pereira, F., Aloisio, G. & Di Marco, A. 2008 Statistical properties of wall pressure fluctuations over a forward-facing step. *Physics of Fluids* **20** (7), 075113.

Castro, I. & Dianat, M. 1983 Surface flow patterns on rectangular bodies in thick boundary layer. *Journal of Wind Engineering and INdustrial Aerodynamics* **11**, 107–119.

Farabee, T. & Casarella, M. 1986*a* Measurments of fluctuating wall pressure for separated/reattached boundary layer flows. *Journal of Vibration, Acoustics, Stress and Reliability in Design* **108**, 301–307.

Farabee, T. M. & Casarella, M. J. 1986*b* Measurements of fluctuating wall pressure for separated/reattached boundary layer flows **108**, 301–307.

Hillier, R. & Cherry, N. J. 1981 The effects of stream turbulence on separation bubbles. *Journal of wind engineering and industrial aerodynamics* **8** (1-2), 49–58.

Keirsbulck, L., Fourrié, G., Labraga, L. & Gad-el Hak, M. 2012 Scaling of statistics in wall-bounded turbulent flows. *Comptes rendus Mécanique.* **340** (6), 420–433.

Kerhervé, F., Jordan, P., Cavalieri, A. V. G., Delville, J., Bogey, C. & Juvé, D. 2012 Educing the source mechanism associated with downstream radiation in subsonic jets. *Journal of Fluid Mechanics* **710**, 606–640.

Lanzerstorfer, D. & Kuhlmann, H. C. 2012 Three-dimensional instability of the flow over a forward-facing step. *Journal of Fluid Mechanics* **695**, 390.

Largeau, J. & Moriniere, V. 2007 Wall pressure fluctuations and topology in separated flows over a forward facing step. *Experiments in Fluids* **21**, 21–40.

Leclercq, D. J. J., Jacob, M. C., Louisot, A. & Talotte, C. 2001 Forward-backward facing step pair: aerodynamic flow, wall pressure and acoustic characterisation. *AIAA paper* **2249**, 2001.

Murray, N. E. & Ukeiley, L. S. 2003 Estimation of the flowfield from surface pressure measurements in an open cavity. *AIAA journal* **41** (5), 969–972.

Pearson, D. S., Goulart, P. J. & Ganapathisubramani, B. 2013 Turbulent separation upstream of a forward-facing step. *Journal of Fluid Mechanics* **724**, 284–304.

Ren, H. & Wu, Y. 2011 Turbulent boundary layers over smooth and rough forward-facing steps. *Physics of Fluids* **23** (045102).

Sherry, M., Lo Jacono, D. & Sheridan, J. 2010 An experimental investigation of the recirculation zone formed downstream of a forward facing step. *Journal of Wind Engineering and Industrial Aerodynamics* **98**, 888–894.

Sherry, M. J., Lo Jacano, D., Sheridan, J., Mathis, R. & Marusic, I. 2009 Flow separation characterization of a forward facing step immersed in a turbulent boundary layer. pp. 1325–1330.

Stüer, H., Gyr, A. & Kinzelbach, W. 1999 Laminar separation on a forward facing step. *European Journal of Mechanics-B/Fluids* **18** (4), 675–692.